Title
A New Anion Receptor for Improving the Interface between Lithium- and Manganese-Rich Layered Oxide Cathode and the Electrolyte

Journal
Chemistry of Materials, 29(5)

ISSN
0897-4756

Authors
Ma, Yulin
Zhou, Yan
Du, Chunyu
et al.

Publication Date
2017-03-14

DOI
10.1021/acs.chemmater.6b04784

Peer reviewed

CHEMISTRY OF MATERIALS

Article

pubs.acs.org/cm

A New Anion Receptor for Improving the Interface between Lithium- and Manganese-Rich Layered Oxide Cathode and the Electrolyte

Yulin Ma,[*,†,‡] Yan Zhou,[†] Chunyu Du,[†] Pengjian Zuo,[†] Xinqun Cheng,[†] Lili Han,[§] Dennis Nordlund,[∥] Yunzhi Gao,[†] Geping Yin,[†] Huolin L. Xin,[§] Marca M. Doeff,[‡] Feng Lin,[‡,⊥] and Guoying Chen[*,‡]

[†]MIIT Key Laboratory of Critical Materials Technology for New Energy Conversion and Storage, School of Chemistry and Chemical Engineering, Harbin Institute of Technology, Harbin 150001, China

[‡]Energy Storage & Distributed Resources Division, Lawrence Berkeley National Laboratory, Berkeley, California 94720, United States

[§]Center for Functional Nanomaterials, Brookhaven National Laboratory, Upton, New York 11973, United States

[∥]Stanford Synchrotron Radiation Lightsource at SLAC, Menlo Park, California 94025, United States

[⊥]Department of Chemistry, Virginia Tech, Blacksburg, Virginia 24061, United States

Supporting Information

ABSTRACT: Surface degradation on cycled lithium-ion battery cathode particles is governed not only by intrinsic thermodynamic properties of the material but also, oftentimes more predominantly, by the side reactions with the electrolytic solution. A superior electrolyte inhibits these undesired side reactions on the cathode and at the electrolyte interface, which consequently minimizes the deterioration of the cathode surface. The present study investigates a new boron-based anion receptor, tris(2,2,2-trifluoroethyl)-borate (TTFEB), as an electrolyte additive in cells containing a lithium- and manganese-rich layered oxide cathode, $Li_{1.16}Ni_{0.2}Co_{0.1}Mn_{0.54}O_2$. Our electrochemical studies demonstrate that the cycling performance and Coulombic efficiency are significantly improved because of the additive, in particular, under elevated temperature conditions. Spectroscopic analyses revealed that the addition of 0.5 wt % TTFEB is capable of reducing the content of lithium-containing inorganic species within the cathode-electrolyte interphase layer and minimizing the reduction of tetravalent Mn^{4+} at the cathode surface. Our work introduces a novel additive highly effective in improving lithium-ion battery performance, highlights the importance in preserving the surface properties of cathode materials, and provides new insights on the working mechanism of electrolyte additives.

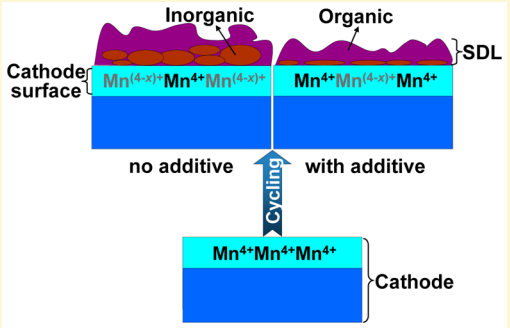

1. INTRODUCTION

Significant progress has been made in lithium-ion batteries (LIBs) for applications in electric vehicles and grid energy storage. The deep market penetration of the LIB technology would be greatly accelerated if methods to further increase energy density, stability and cycle life can be identified and developed.[1] Although intensively studied in the last several decades, cathode materials are still considered a major limiting factor in LIB performance. Over the last 10 years, remarkable efforts have been dedicated to studying a family of lithium- and manganese-rich layered oxides, with a general formula of $Li_{1+x}M_{1-x}O_2$ (where M = Mn, Ni, Co, etc.; such compounds are hereafter referenced as LMR-NMCs).[2−6] Depending on the composition, the oxides can deliver capacities exceeding 250 mAh/g at an average charging voltage of ∼3.6 V vs Li^+/Li. While they have the potential to drastically improve the energy density of lithium-ion batteries, there are several critical problems that prevent their adoption in commercial batteries, including a large first-cycle irreversible capacity loss associated with the activation process, subsequent-cycle voltage decay characterized by a continuous decrease in average discharge voltage along cycling, transition-metal dissolution into the electrolyte, sluggish kinetics, and a high impedance at low state of charge (SOC).

In addition, the high operating voltage of the oxides, along with the catalytic properties of the high-valent transition metals in the charged cathode, degrade the electrolyte by oxidizing the carbonate solvents and decomposing the salt.[7−10] These reactive interactions between the electrode and the electrolyte, or side reactions, not only leave surface deposits onto the cathode, and produce a cathode−electrolyte interphase (CEI) layer, they also modify the intrinsic properties, particularly structural, elemental, and chemical compositions, of the cathode surface itself.[11] While the properties of resulted CEI, much like the solid electrolyte interphase (SEI) at the anode, is influenced by the chemical nature (both organic and inorganic) and the distribution of the side reaction products,[12] studies have shown that a buildup of CEI can increase the charge transfer resistance and deteriorate electrochemical performance.[10] Furthermore, the modification on the surface may lead

Received: November 9, 2016
Revised: February 15, 2017
Published: February 15, 2017

DOI: 10.1021/acs.chemmater.6b04784
Chem. Mater. 2017, 29, 2141−2149

to cathode structural rearrangement that increases the impedance and reduces accessible capacity, both of which reduces usable energy of the cell.[11] The ability of electrolyte additives in influencing the CEI and battery performance has been well-documented in the literature, including many boron-based anion receptors.[13−16] For example, it was reported that anion receptors capable of dissolving electrolyte decomposition byproducts, such as LiF, Li_2O, and Li_2O_2, improve the long-term cycling of LIBs.[17−19] To date, however, most studies have focused on the compositional engineering of additives and the understanding of how electrolyte additives influence the CEI layer. However, the general knowledge on the effect of electrolyte additives on the changes occurring at the cathode particle surface is very limited. Such studies would have a profound impact on additive development that not only benefits the electrolyte community but also the cathode community.

Herein, we report a novel boron-based anion receptor, tris(2,2,2-trifluoroethyl) borate (TTFEB), as an electrolyte additive and investigate its role in the electrochemical performance of $Li_{1.16}Ni_{0.2}Co_{0.1}Mn_{0.54}O_2$/Li half-cells. TTFEB was chosen because of the number of F function groups on the compound. As F is an electron-donating group, we can expect TTFEB to have higher oxidation potential and therefore better anionic stability than the previously reported boron based additives, such as tris(trimethylsilyl) borate (TMSB)[20] and triethylborate (TEB).[21] Indeed, we show that, in the presence of only a small amount of TTFEB additive, both the formation of resistive inorganic deposits species at the interphase and the reduction of transition metal on the cathode surface were significantly reduced, even at an elevated temperature of 55 °C. This led to much-improved practical discharge capacity, cycle life, and Coulombic efficiency of the cells.

2. EXPERIMENTAL SECTION

2.1. Preparation. Tris(2,2,2-trifluoroethyl) borate (TTFEB, 98%) was purchased from Sigma−Aldrich (Shanghai) Trading Co., Ltd. Battery-grade ethylene carbonate (EC) and dimethyl carbonate (DMC) were purchased from Dongguan Shanshan Battery Materials Co., Ltd. (China) and dehydrated by adding 4A molecular sieves. After that, a base electrolyte with 1.0 M $LiPF_6$ (Dongguan Shanshan Battery Material Co., Ltd.) in EC/DMC = 1:2 (volume ratio) was prepared. Another electrolyte with 0.5 wt % TTFEB added to the base electrolyte was also prepared.

$Li_{1.16}Ni_{0.2}Co_{0.1}Mn_{0.54}O_2$ (LNCMO) cathode materials were provided as powder by Coslight Co., Ltd. (Harbin, China). Electrodes were prepared by coating the slurry, consisting of LNCMO (80 wt %), carbon black (10 wt %, Coslight, Harbin), and polyvinylidene fluoride (PVDF) binder (10 wt %, Coslight, Harbin) in *N*-methyl-pyrrolidone (NMP) solvent, onto an Al foil. Afterward, the electrode sheet was dried under vacuum at 120 °C for 8 h. Cathode disks (14 mm in diameter) were punched out, calendared to make dense electrodes, and then assembled into CR2025-type coin cells in an argon-filled glovebox, with metallic lithium as both anode and the reference electrode. Typical active material loading on the cathode is 2 mg/cm^2. Celgard 2500 membrane was used as the separator. Either 1.0 M $LiPF_6$ in EC/DMC (1:2) base electrolyte or the new electrolyte with the addition of 0.5 wt % TTFEB was used.

2.2. Characterization. The crystalline phase in the as-received LNCMO powder was characterized by powder X-ray diffraction (XRD, Empyrean) equipped with a Cu Kα radiation. Morphological features were evaluated via field-emission scanning electron microscopy (FESEM) (FEI Helios Nanolab600i) operating at 30 keV. Chemical composition analysis was performed using inductively coupled plasma−atomic emission spectroscopy (ICP-AES) (Perkin−Elmer Optima 5300DV).

Electrochemical stability of the base electrolyte and TTFEB-added electrolyte were measured by using linear sweep voltammetry (LSV) in a three-electrode cell, in which Pt foil was used as the working electrode and metallic lithium foils as reference and counter electrodes. Electrochemical workstation impedance analyzer (PARSTAT2273) was used to measure the electrochemical impedance spectroscopy (EIS) in a frequency range of 10 mHz to 100 kHz with an amplitude of 10 mV. The electrochemical performance of $Li_{1.16}Ni_{0.2}Co_{0.1}Mn_{0.54}O_2$/ Li coin cells was tested galvanostatically on a Neware BTS instrument over the range of 2.0−4.8 V at a 1C or C/2 rate, each after three formation cycles at C/10 at either 25 or 55 °C. C/10, C/2, and 1C correspond to current densities of 25, 125, and 250 mA/g, respectively. After 100 cycles at 55 °C in either type of electrolytic solution, LNCMO electrodes were then removed from coin cells, rinsed with DMC to remove any residual salt, and allowed to dry in the glovebox at room temperature.

The composition of surface deposits on cycled LNCMO electrodes were measured by X-ray photoelectron spectroscopy (XPS) (PHI 5700 ESCA system) with Al Kα radiation ($h\nu$ = 1486.6 eV) as the X-ray light source. The energy scale was calibrated by the C 1s peak at 284.6 eV and then fitted by XPS peak software. Soft X-ray absorption spectroscopy (XAS) measurements were performed on the bending magnet beamline 8-2 at Stanford Synchrotron Radiation Lightsource (SSRL). A ring current of 500 mA and a 1,100 l mm^{-1} spherical grating monochromator with 20 μm entrance and exit slits were used, providing ~0.5 × 10^{10} ph s^{-1} at 0.2 eV resolution in a 1 mm^2 beam spot. Samples were mounted onto an aluminum sample holder with double-sided carbon tape in an argon-filled glovebox and then transferred to the load-lock chamber in an airtight container, using a glovebag purged with argon for the transfer. Data were acquired under ultrahigh vacuum (10^{-9} Torr) in a single load at room temperature using total electron yield (TEY), where the sample drain current was collected. All spectra were normalized by the current from a gold evaporated fine grid positioned upstream of the main chamber. Two probe-corrected field-emission scanning transmission electron microscopy (STEM) systems operating at 200 and 300 keV were used for annular dark-field scanning transmission electron microscopy (ADF-STEM) imaging and spatially resolved electron energy loss spectroscopy (EELS) measurements. Cathode particles were collected by scratching the cycled electrode (after 100 cycles at 55 °C) and then deposition onto TEM grids for the study.

3. RESULTS AND DISCUSSION

The structural analysis of the as-received LNCMO material was provided in the XRD pattern (Figure S1 in the Supporting Information), which closely resembles those of LMR-NMCs reported in the literature,[22] suggesting good crystallinity and phase purity of the starting material. The particles were large spheres with an average size of ~10−20 μm, as shown in the SEM image in Figure S2 in the Supporting Information. The anodic stability of the electrolyte with and without the addition of 0.5 wt % TTFEB was compared by using linear sweep voltammetry, and the results are shown in Figure S3 in the Supporting Information. Prior to 4.8 V, no obvious current was detected on the LSV profiles of both electrolytes, which confirms the excellent stability of TTFEB under the oxidative conditions.

The charge−discharge behavior of the LNCMO cells with and without the additive was compared to investigate the influence of TTFEB on electrochemical performance. Figure 1a shows the room-temperature cycling performance of the LNCMO half-cells cycled at 1C between 2.0 and 4.8 V, each after the first three formation cycles at C/10. Both cells delivered a discharge capacity of 230−240 mAh/g at C/10, which decreased to ~140−150 mAh/g at 1C, indicating that TTFEB additive has good compatibility with the system. Upon long-term cycling at 1C, the capacity retention was much better

DOI: 10.1021/acs.chemmater.6b04784
Chem. Mater. 2017, 29, 2141−2149

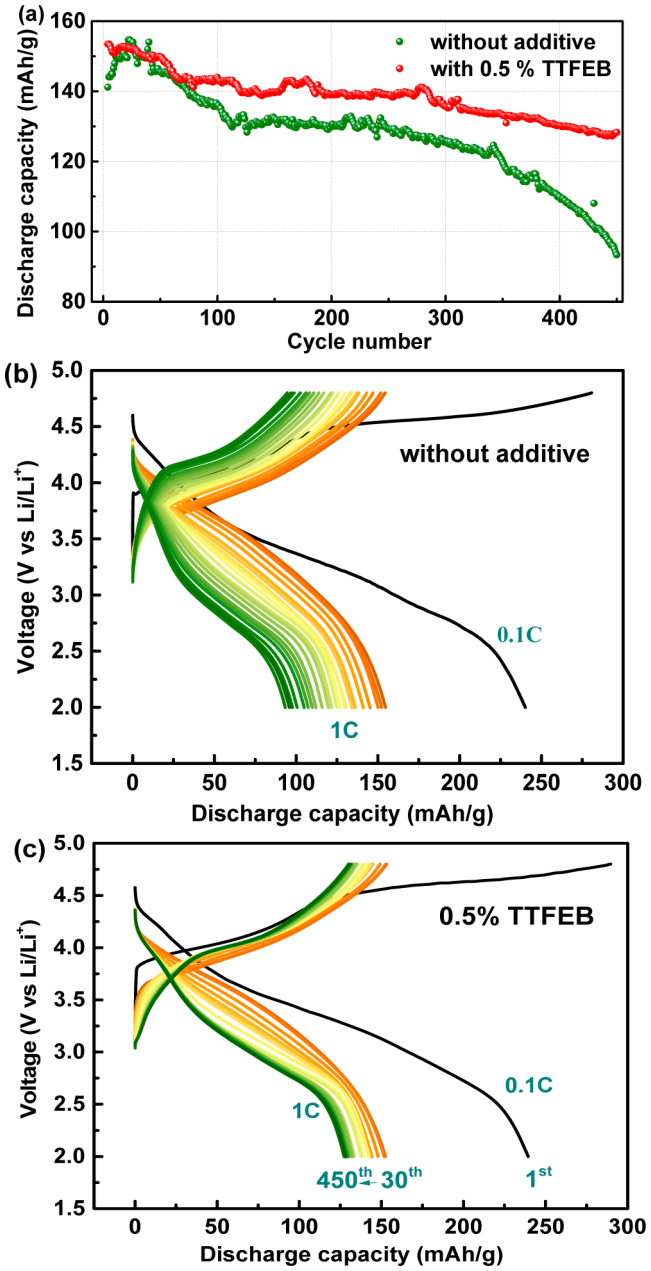

Figure 1. (a) Room-temperature discharge capacity as a function of cycle number in $Li_{1.16}Ni_{0.2}Co_{0.1}Mn_{0.54}O_2$ half-cells with and without the presence of 0.5 wt % TTFEB additive, (b) 1C rate charge–discharge profiles of the half-cell without the additive (every 30th cycle shown) between 2.0–4.8 V, after three cycles at C/10 (only the first cycle shown), and (c) 1C rate charge–discharge profiles of the half-cell with 0.5% TTFEB additive (every 30th cycle shown) between 2.0 and 4.8 V, after three cycles at C/10 (only the first cycle shown).

in the cell with 0.5 wt % TTFEB, where a discharge capacity of 130 mAh/g was obtained after 460 cycles (or 14% capacity loss). In contrast, the discharge capacity decreased to 90 mAh/g, or 40% capacity loss, without the additive. The charge–discharge profiles, as a function of cycle number for the cells without and with the additive, are shown in Figures 1b and 1c, respectively. The first charging curve at C/10 is composed of a sloping region (up to 4.5 V) and a plateau region (~4.5 V). The charging voltage region below 4.5 V is typically attributed to lithium-ion extraction from the lithium layer in LNCMO and the redox processes involving Ni^{2+} and possibly, Co^{3+}.[23−25] The subsequent voltage plateau at ~4.5 V involves the activation of the cathode material which extracts Li from the transition metal layer, together with oxygen release and structural rearrangements.[26] The evolution of oxygen gas in this region is likely to promote the formation of higher dielectric inorganic compounds, such as Li_2O, Li_2CO_3, and LiF, in the CEI.[27] Careful analysis of Figures 1b and 1c also suggests that, in the absence of TTFEB additive, the polarization in the LNCMO cell increased more rapidly upon cycling, signaling more-extensive modification in this case.

Reliable battery performance at elevated temperature is important for many practical applications. However, side reactions between the cathode and the electrolyte are usually more severe under these conditions. In addition, it was reported that structural transformation resulting from the redox activities of Mn in Li- and Mn-rich layered oxides is significantly enhanced.[28] Figure 2a shows the discharge capacity retention

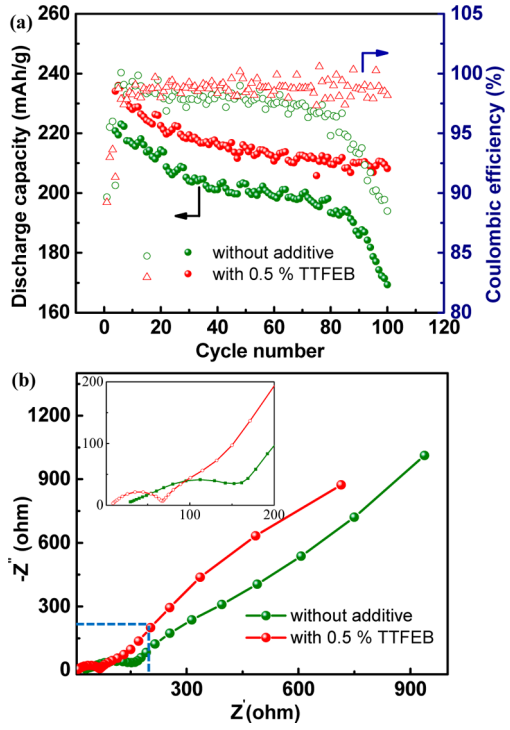

Figure 2. (a) Cycling performance and Coulombic efficiency of LNCMO half cells cycled at C/2 between 2.0–4.8 V at 55 °C and (b) electrochemical impedance spectra of fully discharged LNCMO/Li cells after 90 cycles at 55 °C (inset shows a magnified region of the low-frequency region). The first three formation cycles at C/10 are not shown in panel (a).

and Coulombic efficiency of the LNCMO/Li cells cycled at C/2 at 55 °C with and without 0.5 wt % TTFEB, after first three formation cycles at C/10. The charge–discharge profiles as a function of cycle number for the cells with and without the additive are shown in Figure S4 in the Supporting Information. In the cell without the electrolyte additive, the discharge capacity decreased from 220 mAh/g to 169 mAh/g (~23% capacity loss) and the Coulombic efficiency dropped to 88.5% after only 100 cycles. In contrast, after the same number of cycles, the discharge capacity was 210 mAh/g (~5% capacity loss) and the Coulombic efficiency maintained above 98% in the cell with the additive. Clearly, the addition of 0.5 wt % TTFEB to the electrolytic solution is highly beneficial to the

DOI: 10.1021/acs.chemmater.6b04784
Chem. Mater. 2017, 29, 2141−2149

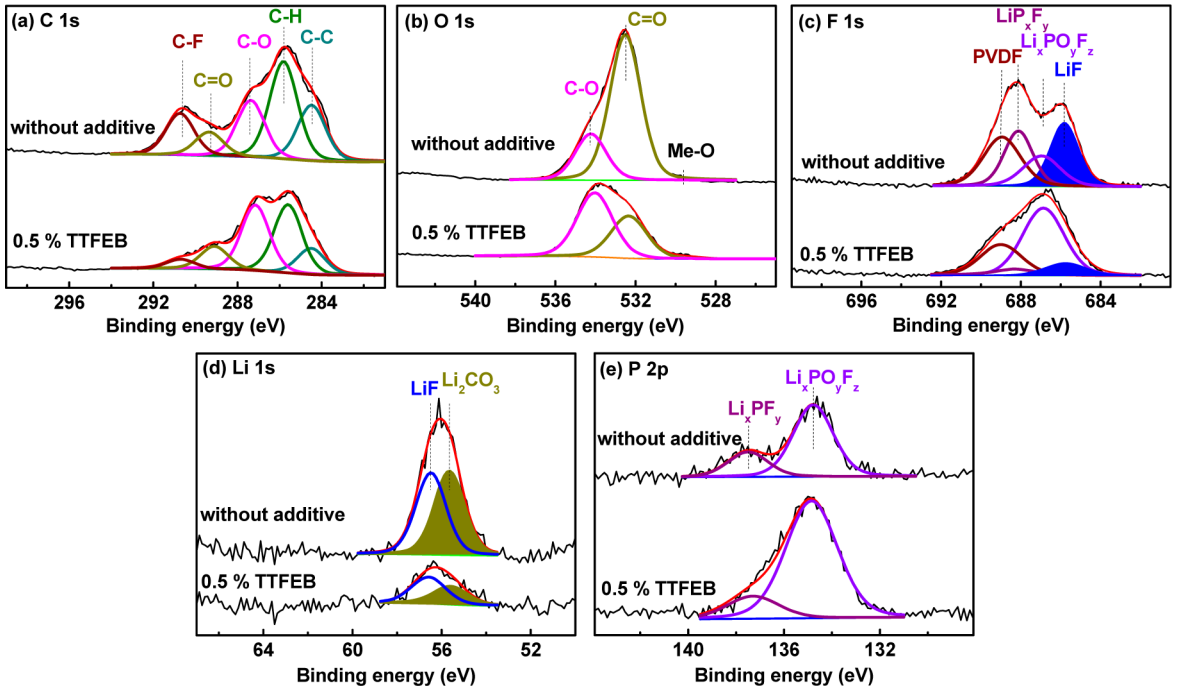

Figure 3. XPS spectra of (a) C 1s, (b) O 1s, (c) F 1s, (d) Li 1s, and (e) P 2p of the recovered LNCMO electrodes cycled 100 times at 55 °C in an electrolyte with or without 0.5 wt % TTFEB.

cell performance at elevated temperatures. The charge and discharge average voltages during long-term cycling at both room temperature and 55 °C are shown in Figure S5 in the Supporting Information. Without the additive, there is a gradual increase in average charge voltage and decrease in discharge voltage upon cycling at both room temperature and elevated temperature, consistent with the severe voltage decay typically observed in Li- and Mn-rich layered oxide cathodes. In the presence of TTFEB, however, the average charge and discharge voltage became much more stable upon cycling, indicating that the additive is beneficial for voltage stabilization of LNCMO cathode material.

We also investigated the electrochemical impedance spectroscopy of the LNCMO/Li cells after 30 and 90 cycles at 55 °C, both discharged to 2.0 V, and the results are shown in Figure S6a in the Supporting Information, as well as Figure 2b. Based on the previous reports, the high-frequency semicircle can be attributed to surface layer resistance (R_{sf}) and capacitance (C_{sf}), a medium-to-low-frequency semicircle arise from the charge transfer resistance (R_{ct}) and double layer capacitance (C_{dl}), and a low-frequency Warburg impedance (Z_w) is due to solid-state diffusion of lithium ions within the active material.[29,30] By fitting the equivalent circuit shown in Figure S6b, the value of R_{sf} for pristine material, after 30 and 90 cycles at 55 °C, was obtained and compared in Table S1 in the Supporting Information. While the R_{sf} value of pristine material was determined to be ∼23 and 39 Ω in the cells with and without the additive, it increased to ∼61 Ω and 94 Ω after 30 cycles, respectively. After 90 cycles, it increased to ∼129 Ω (37% increase) in the cell without the additive while maintained at 61 Ω in cell with the additive. The results clearly suggest that the addition of TTFEB reduces the buildup of the surface resistance associated with cell cycling. The trend in impedance rise, higher in the early cycles compared to the later cycles, is also consistent with the impact of the additive on the formation of Li_2CO_3 and LiF, both of which are expected to be more severe in the early cycles.

To investigate the reasons behind the positive effect of the electrolyte additive, we first performed experiments to rule out the contribution of significant impedance growth at the Li metal anode. After collecting the EIS data of the LNCMO half cells cycled with and without the additive, the cathodes were removed without rinsing and reassembled into new cells with a fresh Li metal electrode and fresh electrolyte with and without additive, respectively. EIS measurements were performed on the new cells, which showed that the impedance of both cells decreased slightly, compared to the corresponding cycled cell, indicating a small contribution of impedance growth at Li anode in the cycled cells. Even in the freshly assembled new cells, the surface impedance of the cathodes cycled without the additive is significantly larger than that with TTFEB, suggesting that the main cause of capacity fade is at the cathode. We then recovered the cathodes after 100 cycles at 55 °C and analyzed them using the surface-sensitive XPS technique, which typically probe the top ∼2−3 nm of the surface. The elemental concentration at the electrode surface is listed in Table S2 in the Supporting Information. In both cases, there is an increase in the Ni/Co ratio from the bulk value of 2, suggesting possible surface Ni segregation, along with cycling, which is a phenomenon that has been previously reported in this class of materials.[31] In the presence of the additive, the Li concentration was noticeably lower, indicating that TTFEB indeed reduces the overall content of lithium-containing compounds on the surface. Meanwhile, boron was not detected on the surface of the electrode, confirming that TTFEB was stable during cycling, as evidenced by the LSV study. Figure 3 shows the chemical-environment-sensitive XPS spectra for the various non-transition-metal elements identified on the CEI layer. In the C 1s spectra (Figure 3a), C−C (284.9 eV) originates from super-P in the electrodes, C−H (285.7 eV) and C−F (290.5 eV) are characteristic of PVDF binder,[32] C−O

DOI: 10.1021/acs.chemmater.6b04784
Chem. Mater. 2017, 29, 2141−2149

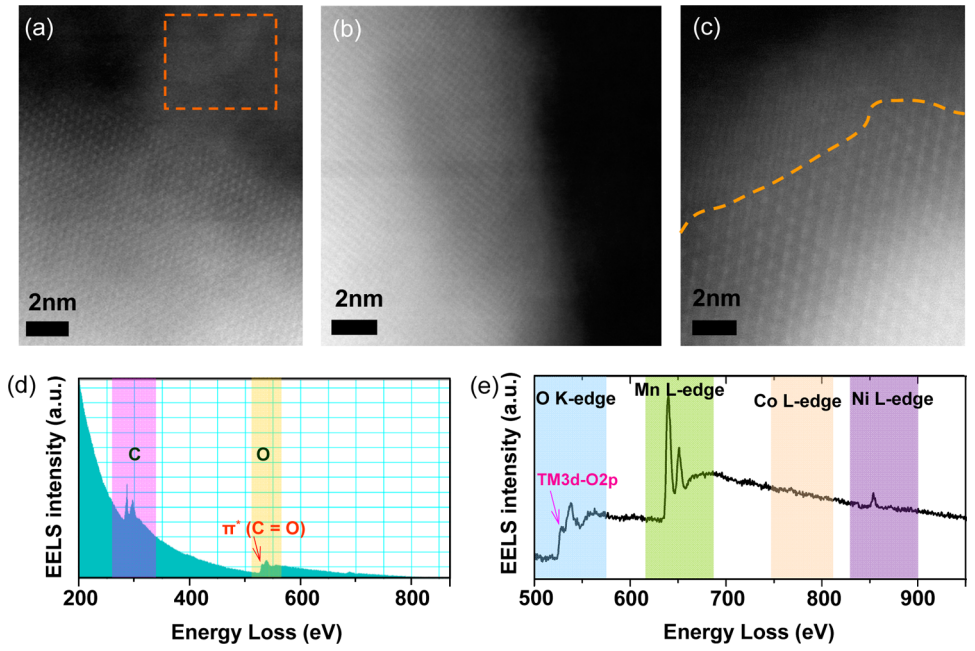

Figure 4. (a, b, c) STEM images showing the surface of LNCMO cathode particles recovered from the cell after 100 cycles at 55 °C in the presence of the additive, (d) C K-edge and O K-edge EELS data collected from the selected area in panel (a), and (e) O K-edge, Mn L-edge, and Ni L-edge EELS data collected from the entire region of panel (b).

(286.8 eV) is indicative of PEO-like oligomers,[33,34] and C═O (288.05 eV) is likely from lithium alkyl carbonates (such as $ROCO_2Li$) and Li_2CO_3.[33] The intensity of C−O increases while C═O drops when 0.5 wt % TTFEB was added, indicating that TTFEB reduces the formation of lithium alkyl carbonates and Li_2CO_3 but it does not eliminate them. This is also supported by the O 1s spectra (Figure 3b), where the carbonates are shown to be more dominating in the absence of the additive.[33] Furthermore, the intensity of LiF (685.8 eV)[35] on the F 1s spectra decreased significantly with the additive, confirming that TTFEB is indeed capable of reducing the formation of LiF at the interphase between LNCMO cathode and the electrolyte. The Li 1s spectra in Figure 3d further verifies lower concentration of both Li_2CO_3 (55.7 eV)[38] and LiF (56.5 eV)[36] and provides additional evidence that TTFEB reduces insulating inorganic byproducts at the interphase. On the other hand, the addition of the additive led to a higher concentration of LiP_xF_y (688.1 eV) and $Li_xPO_yF_z$ (687.0 eV), two of the most common decomposition products from $LiPF_6$-containing electrolyte, on the cycled cathode surface (Figure 3c). The result is also confirmed by the P 2p spectra shown in Figure 3e. A plausible explanation is the ability of the boron-based anion receptor in coordinating with $LiPF_6$ and accelerating its decomposition, as described in the previous reports.[36,37] Similar to other boron-based anion receptors, the B atom in TTFEB is highly electrophilic and electron-deficient with strong electron-withdrawing capability.[39,40] This may assist with the dissolution of lithium salts by interacting with their anions, such as F^-. It is conceivable that because of this enhanced activity, the accumulation of nonconductive, inorganic lithium-containing compounds on electrode surface was significantly reduced.

The decomposition of the electrolyte is likely accompanied by transition-metal reduction on the cathode surface. This further alters the electrode−electrolyte interphase and promotes structural transformation in the bulk of the oxides, both of which have a detrimental effect on the cycling performance of the cathodes, particularly during the high-voltage operation.[11,41−46] To this end, we used both spatially resolved and ensemble-averaged spectroscopic techniques to investigate the nature of the surface transition metals on particles cycled with and without the additive. First, spatially resolved STEM-EELS technique was used to characterize the CEI layer and the chemical state of the surface transition metals on the cathode cycled in the presence of TTFEB. The EELS data (Figure 4d), collected from the selected area in the red square covering the CEI region only (Figure 4a), confirms that the surface deposits indeed contain carbonates,[44] as shown by the XPS analysis. We then collected the EELS data (Figure 4e) from the entire area in the STEM image shown in Figure 4b that includes the surface of the cycled particle. All three transition metals were detected, although the signal of Co L-edge was significantly lower, compared to that of the Mn L-edge and the Ni L-edge. This is likely due to the inherently low Co concentration in the material, as well as possible surface Ni enrichment, consistent with the observation in XPS. O K-edge EELS corresponding to the transition from O 1s states to unoccupied O 2p states has been used to study the average oxidation states of the transition metals, because of the strong hybridization between transition metals and oxygen in the layered structure.[41,42,46] Also, the intensity of the pre-edge peak in the O K-edge is usually in a positive relationship with the formal oxidation states of Ni, Mn, and Co, because of the sharing of hole states in the $(TM)O_6$ units. We found that the intensity of the pre-edge peak observed on the cycled LNCMO (Figure 4e) was significantly lower, compared to what was reported on similar compounds in the literature,[44] suggesting an overall reduction in oxidation states of the transition metals. The surface transition metal reduction in lithium- and manganese-rich transition metal oxides usually involves structural rearrangement from the layered phase to a less-ordered phase, such as spinel or rock-salt. This was indeed

DOI: 10.1021/acs.chemmater.6b04784
Chem. Mater. 2017, 29, 2141−2149

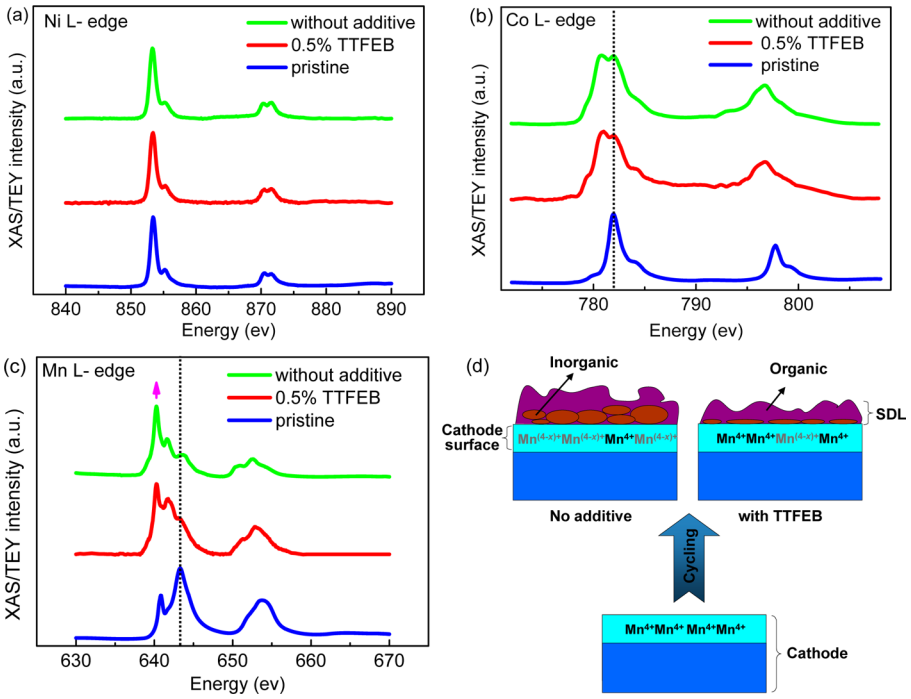

Figure 5. (a) Ni L-edge, (b) Co L-edge, (c) Mn L-edge TEY-XAS spectra of pristine and recovered cathodes after 100 cycles at 55 °C with and without TTFEB additive, and (d) schematic diagram of the cathode and electrolyte interphase with and without the additive. For simplicity, only Mn cations are shown on the cathode surface. All spectra were normalized to the highest peak in the pattern.

captured by the high-resolution STEM imaging in a different zone axis (Figure 4c) which shows structural densification in the surface region and the lack of the layered structure on the cycled particle surface, similar to what was reported in our previous paper.[47]

In order to provide a statistically viable comparison between the electrodes cycled with and without the electrolyte additive, XAS, which is an ensemble-averaged technique, was then used to study the oxidation state changes of transition metals in a large number of particles (~10^7 particles). The total electron yield (TEY) mode of soft XAS reveals the chemical information on the transition metals at the surface layer of electrodes, in the region of ~5 nm deep.[42] Here, we studied cycling-induced changes in the L-edges of Ni, Co, and Mn. The absorption peaks of the metal L-edge XAS are relatively intense, because of the electric dipole-allowed 2p → 3d transition, which is sensitive to the oxidation state of the studied metal and the covalency of the metal−oxygen bonds.[48] XAS spectra of cycled and pristine LNCMO are shown in Figure 5. After 100 cycles at 55 °C, no obvious difference was observed in Ni L-edge spectra (Figure 5a) as it remained at a 2+ oxidation state. The Co L-edge XAS spectrum of the pristine material (Figure 5b) confirms the oxidation state of Co at 3+, as expected. A significant enhancement in the low-energy peak was found on both cycled samples, regardless of the electrolyte used. As an increase in the low/high energy peak ratio in Co L3-edge region corresponds to a decrease in unoccupied high-energy Co 3d state; the results indicate Co reduction in both cases. Figure 5c shows the Mn L2- and L3-edge XAS spectra where the valence state of Mn in the pristine sample was determined to be 4+, based on the line shape and energy position, compared to the standards.[43] The appearance of the low-energy shoulder peak (near 640 eV) along with the decrease in the intensity of the main L3-peak (near 644 eV) in the cycled samples reveal the dominance of lower-valence manganese species, possibly in Mn^{3+} and/or Mn^{2+}.[49] The intensity ratio between the low-energy shoulder and the high-energy shoulder, however, is significantly lower in the electrode cycled with the additive, confirming the ability of the additive in stabilizing the surface and minimizing the reduction of surface transition metal (in this case, Mn).

Figure 5d shows the schematic for the evolution of the cathode and electrolyte interphase during long-term cycling. In the presence of the additive, the overall content of Li-containing compounds in the surface deposit layer (SDL) was reduced as evidenced by the lower Li concentration in the XPS spectra. Moreover, the presence of the insulating inorganic components, particularly LiF and Li_2CO_3, was also reduced, yielding phosphorus-containing species such as LiP_xF_y and $Li_xPO_yF_z$. This likely promotes more free movement of Li ions and electrons, better utilization of the cathode material, and overall higher capacity. It is commonly believed that, in LMR-NMCs, surface Mn reduction precedes bulk structural transformation from a layered phase to a spinel-type phase, which is responsible for a range of performance-limiting issues experienced by these oxides. A decrease in Mn reduction also helps to stabilize the cathode structure and the cathode and electrolyte interphase by minimizing the attack of chemicals like HF on the lower-valent Mn that leads to its eventual dissolution into the electrolyte. This was confirmed by the studies performed on the recovered separators and Li anodes from the LNMCO half-cells cycled 100 times at 55 °C. Figure S7 in the Supporting Information compares the SEM images of separators. While the separator obtained from the cell cycled with the additive showed an almost-pristine condition, particularly deposits, which are shown as bright spots on the image, was clearly seen on the one recovered from the cell without the TTFEB additive. Table S3 shows the content of Mn, Ni, and Co deposited on Li foils determined by ICP-MS. The cycled lithium metal anodes were washed with DMC for

DOI: 10.1021/acs.chemmater.6b04784
Chem. Mater. 2017, 29, 2141−2149

three times and then dissolved in a 2% HNO_3 solution. The pH of the solution was adjusted to 7 before the measurement. While a small amount of transition metals were found on the lithium anode cycled with the TTFEB, an ~10 times higher concentration was found on the one without the additive. This provides clear evidence that TTFEB inhibits the dissolution of transition metal during cycling. All in all, TTFEB additive positively influences the interactions between the cathode and the electrolyte, which enables a more stable cathode/electrolyte interphase capable of extended battery cycling.

Although all the results shown here are based on the addition of 0.5 wt % of TTFEB, the effect of adding different amounts of additive was also evaluated. Figure S8 in the Supporting Information shows the capacity retention of $Li_{1.16}Ni_{0.2}Co_{0.1}Mn_{0.54}O_2$/Li half-cells with 0.2%, 0.5%, and 1% TTFEB, respectively. Cycling performance was improved by increasing the content from 0.2% to 0.5% but it remained the same from 0.5% to 1%. This is consistent with the literature reports, where most additives showed the best results at ~0.5%−1.0%.[17−21]

4. CONCLUSIONS

We report a new electrolyte additive—tris(2,2,2-trifluoroethyl) borate (TTFEB)—to improve the discharge capacity, Coulombic efficiency, and cycle lives of cells with a high-capacity lithium- and manganese-rich layered cathode. TTFEB suppressed the growth of insulating inorganic byproducts at the cathode/electrolyte interphase, inhibited the growth of resistive surface film, and alleviated the cell polarization during cycling. Furthermore, surface transition metal (mostly Mn) reduction and dissolution was mitigated when the electrode was cycled in a TTFEB-containing electrolyte. From the perspective of electrolyte additive application, our finding expands the collection of anion acceptors for lithium ion batteries and provides insights on additional working mechanisms for their positive effect on cell performance.

■ ASSOCIATED CONTENT

Supporting Information

The Supporting Information is available free of charge on the ACS Publications website at DOI: 10.1021/acs.chemmater.6b04784.

Powder XRD pattern of the LNCMO material, linear sweep voltammetry of a Pt working electrode in different electrolytes, EIS of the LNCMO/Li cells, SEM image of the pristine LNCMO material, surface resistance (R_{sf}) obtained by fitting the equivalent circuit, elemental concentration detected on the surface of LNCMO electrodes (PDF)

■ AUTHOR INFORMATION

Corresponding Authors

*E-mail: mayulin@hit.edu.cn.
*E-mail: gchen@lbl.gov.

ORCID

Geping Yin: 0000-0002-8804-6550
Feng Lin: 0000-0002-3729-3148
Guoying Chen: 0000-0002-3218-2609

Author Contributions

The manuscript was written through contributions of all authors.

Notes

The authors declare no competing financial interest.

■ ACKNOWLEDGMENTS

This work was supported by the National Science Foundation of China (Nos. 51202047 and 21373072), the Heilongjiang Postdoctoral Fund (No. LBH-Z11141) and China Scholarship Council. We would like to acknowledge the support by the Assistant Secretary for Energy Efficiency and Renewable Energy, Office of FreedomCAR and Vehicle Technologies of the U.S. Department of Energy (under Contract No. DE-AC02-05CH11231). This research used the Hitachi dedicated STEM of the Center for Functional Nanomaterials, which is a U.S. Department of Energy Office of Science Facility, at Brookhaven National Laboratory (under Contract No. DE-SC0012704). The synchrotron X-ray portion of this work was carried out at the Stanford Synchrotron Radiation Lightsource, a Directorate of SLAC National Accelerator Laboratory and an Office of Science User Facility operated for the U.S. Department of Energy Office of Science by Stanford University that is supported by the U.S. Department of Energy, Office of Science, and Office of Basic Energy Sciences under Contract No. DE-AC02-76SF00515. F.L. and D.N. would like to thank Dr. J.-S. Lee for the assistance at SSRL beamline 8-2. F.L. gratefully acknowledges Virginia Tech Department of Chemistry startup funds.

■ REFERENCES

(1) Gao, X.-P.; Yang, H.-X. Multi-electron reaction materials for high energy density batteries. *Energy Environ. Sci.* **2010**, *3*, 174−189.

(2) Thackeray, M. M.; Kang, S.-H.; Johnson, C. S.; Vaughey, J. T.; Benedek, R.; Hackney, S. A. Li_2MnO_3-stabilized $LiMO_2$ (M = Mn, Ni, Co) electrodes for lithium-ion batteries. *J. Mater. Chem.* **2007**, *17*, 3112−3125.

(3) Thackeray, M. M.; Johnson, C. S.; Vaughey, J. T.; Li, N.; Hackney, S. A. Advances in manganese-oxide 'composite' electrodes for lithium-ion batteries. *J. Mater. Chem.* **2005**, *15*, 2257−2267.

(4) Yu, H.; Zhou, H. High-energy cathode materials (Li_2MnO_3−$LiMO_2$) for lithium-ion batteries. *J. Phys. Chem. Lett.* **2013**, *4*, 1268−1280.

(5) Liu, H.; Chen, C.; Du, C.; He, X.; Yin, G.; Song, B.; Zuo, P.; Cheng, X.; Ma, Y.; Gao, Y. Lithium-rich $Li_{1.2}Ni_{0.13}Co_{0.13}Mn_{0.54}O_2$ oxide coated by Li_3PO_4 and carbon nanocomposite layers as high performance cathode materials for lithium ion batteries. *J. Mater. Chem. A* **2015**, *3*, 2634−2641.

(6) Liu, H.; Du, C.; Yin, G.; Song, B.; Zuo, P.; Cheng, X.; Ma, Y.; Gao, Y. A Li-rich oxide cathode material with mosaic spinel grain and a surface coating for high performance Li-ion batteries. *J. Mater. Chem. A* **2014**, *2*, 15640−15646.

(7) Armstrong, A. R.; Holzapfel, M.; Novák, P.; Johnson, C. S.; Kang, S. H.; Thackeray, M. M.; Bruce, P. G. Demonstrating oxygen loss and associated structural reorganization in the lithium battery cathode $Li[Ni_{0.2}Li_{0.2}Mn_{0.6}]O_2$. *J. Am. Chem. Soc.* **2006**, *128*, 8694−8698.

(8) Yabuuchi, N.; Yoshii, K.; Myung, S. T.; Nakai, I.; Komaba, S. Detailed studies of a high-capacity electrode material for rechargeable batteries, Li_2MnO_3−$LiCo_{1/3}Ni_{1/3}Mn_{1/3}O_2$. *J. Am. Chem. Soc.* **2011**, *133*, 4404−4419.

(9) Hy, S.; Felix, F.; Rick, J.; Su, W. N.; Hwang, B. J. Direct In situ Observation of Li_2O Evolution on Li-Rich High-Capacity Cathode Material, $Li\,[Ni_xLi_{(1-2\,x)/3}Mn_{(2-x)/3}]\,O_2$ ($0 \leq x \leq 0.5$). *J. Am. Chem. Soc.* **2014**, *136*, 999−1007.

(10) Xu, K. Electrolytes and interphases in Li-ion batteries and beyon. *Chem. Rev.* **2014**, *114*, 11503−11618.

(11) Lin, F.; Markus, I. M.; Nordlund, D.; Weng, T.-C.; Asta, M. D.; Xin, H. L.; Doeff, M. M. Surface reconstruction and chemical

DOI: 10.1021/acs.chemmater.6b04784
Chem. Mater. 2017, 29, 2141−2149

evolution of stoichiometric layered cathode materials for lithium-ion batteries. *Nat. Commun.* **2014**, *5*, 3529.
(12) Shi, F.; Ross, P. N.; Zhao, H.; Liu, G.; Somorjai, G. A.; Komvopoulos, K. A Catalytic Path for Electrolyte Reduction in Lithium-Ion Cells Revealed by *In Situ* Attenuated Total Reflection-Fourier Transform Infrared Spectroscopy. *J. Am. Chem. Soc.* **2015**, *137*, 3181−3184.
(13) Xu, M.; Tsiouvaras, N.; Garsuch, A.; Gasteiger, H.; Lucht, B. L. Generation of cathode passivation films via oxidation of lithium bis (oxalato) borate on high voltage spinel ($LiNi_{0.5}Mn_{1.5}O_4$). *J. Phys. Chem. C* **2014**, *118*, 7363−7368.
(14) Zhang, L.; Ma, Y.; Cheng, X.; Zuo, P.; Cui, Y.; Guan, T.; Du, C.; Gao, Y.; Yin, G. Enhancement of high voltage cycling performance and thermal stability of $LiNi_{1/3}Co_{1/3}Mn_{1/3}O_2$ cathode by use of boron-based additives. *Solid State Ionics* **2014**, *263*, 146−151.
(15) Bouayad, H.; Wang, Z.; Dupré, N.; Dedryvère, R.; Foix, D.; Franger, S.; Martin, J. F.; Boutafa, L.; Patoux, S.; Gonbeau, D.; Guyomard, D. Improvement of electrode/electrolyte interfaces in high-voltage spinel lithium-ion batteries by using glutaric anhydride as electrolyte additive. *J. Phys. Chem. C* **2014**, *118*, 4634−4648.
(16) McBreen, J.; Lee, H. S.; Yang, X. Q.; Sun, X. New approaches to the design of polymer and liquid electrolytes for lithium batteries. *J. Power Sources* **2000**, *89*, 163−167.
(17) Prakash Reddy, V.; Blanco, M.; Bugga, R. Boron-based anion receptors in lithium-ion and metal-air batteries. *J. Power Sources* **2014**, *247*, 813−820.
(18) Zheng, J.; Xiao, J.; Gu, M.; Zuo, P.; Wang, C.; Zhang, J. G. Interface modifications by anion receptors for high energy lithium ion batteries. *J. Power Sources* **2014**, *250*, 313−318.
(19) Zhang, J.; Wang, J.; Yang, J.; Nuli, Y. Artificial interface deriving from sacrificial tris (trimethylsilyl) phosphate additive for lithium rich cathode materials. *Electrochim. Acta* **2014**, *117*, 99−104.
(20) Li, J.; Xing, L.; Zhang, R.; Chen, M.; Wang, Z.; Xu, M.; Li, W. Tris(trimethylsilyl) borate as an electrolyte additive for improving interfacial stability of high voltage layered lithium-rich oxide cathode/carbonate-based electrolyte. *J. Power Sources* **2015**, *285*, 360−366.
(21) Wang, Z.; Xing, L.; Li, J.; Xu, M.; Li, W. Triethylborate as an electrolyte additive for high voltage layered lithium nickel cobalt manganese oxide cathode of lithium ion battery. *J. Power Sources* **2016**, *307*, 587−592.
(22) Chen, G.; Hai, B.; Shukla, A. K.; Duncan, H. Impact of Initial Li Content on Kinetics and Stabilities of Layered $Li_{1+x}(Ni_{0.33}Mn_{0.33}Co_{0.33})_{1-x}O_2$. *J. Electrochem. Soc.* **2012**, *159*, A1543−A1550.
(23) Kang, S. H.; Kim, J.; Stoll, M. E. Layered Li $(Ni_{0.5-x}Mn_{0.5-x}M_{2x})O_2$ (M = Co, Al, Ti; x = 0, 0.025) cathode materials for Li-ion rechargeable batteries. *J. Power Sources* **2002**, *112*, 41−48.
(24) Liu, J.; Hou, M.; Yi, J.; Guo, S.; Wang, C.; Xia, Y. Improving the electrochemical performance of layered lithium-rich transition-metal oxides by controlling the structural defects. *Energy Environ. Sci.* **2014**, *7*, 705−714.
(25) Yu, X.; Lyu, Y.; Gu, L.; Wu, H.; Bak, S. M.; Zhou, Y.; Amine, K.; Ehrlich, S. N.; Li, H.; Nam, K. W.; Yang, X. Q. Understanding the Rate Capability of High-Energy-Density Li-Rich Layered $Li_{1.2}Ni_{0.15}Co_{0.1}Mn_{0.55}O_2$ Cathode Materials. *Adv. Energy Mater.* **2014**, *4*, 1300950.
(26) Shen, C. H.; Wang, Q.; Fu, F.; Huang, L.; Lin, Z.; Shen, S. Y.; Su, H.; Zheng, X. M.; Xu, B. B.; Li, J. T.; Sun, S. G. Facile Synthesis of The Li-Rich Layered Oxide $Li_{1.23}Ni_{0.09}Co_{0.12}Mn_{0.56}O_2$ with Superior Lithium Storage Performance and New Insights into Structural Transformation of the Layered Oxide Material during Charge-Discharge Cycle: *In Situ* XRD Characterization. *ACS Appl. Mater. Interfaces* **2014**, *6*, 5516−5524.
(27) Hong, J.; Lim, H. D.; Lee, M.; Kim, S. W.; Kim, H.; Oh, S. T.; Chung, G. C.; Kang, K. Critical role of oxygen evolved from layered Li-excess metal oxides in lithium rechargeable batteries. *Chem. Mater.* **2012**, *24*, 2692−2697.
(28) Li, Q.; Li, G.; Fu, C.; Luo, D.; Fan, J.; Xie, D.; Li, L. Balancing stability and specific energy in Li-rich cathodes for lithium ion batteries: a case study of a novel Li-Mn-Ni-Co oxide. *J. Mater. Chem. A* **2015**, *3*, 10592−10602.
(29) Liao, L.; Cheng, X.; Ma, Y.; Zuo, P.; Fang, W.; Yin, G.; Gao, Y. Fluoroethylene carbonate as electrolyte additive to improve low temperature performance of $LiFePO_4$ electrode. *Electrochim. Acta* **2013**, *87*, 466−472.
(30) Hai, B.; Shukla, A. K.; Duncan, H.; Chen, G. The effect of particle surface facets on the kinetic properties of $LiMn_{1.5}Ni_{0.5}O_4$ cathode materials. *J. Mater. Chem. A* **2013**, *1*, 759−769.
(31) Yan, P.; Nie, A.; Zheng, J.; Zhou, Y.; Lu, D.; Zhang, X.; Xu, R.; Belharouak, I.; Zu, X.; Xiao, J.; Amine, K.; Liu, J.; Gao, F.; Shahbazian-Yassar, R.; Zhang, J. G.; Wang, C. M. Evolution of lattice structure and chemical composition of the surface reconstruction layer in $Li_{1.2}Ni_{0.2}Mn_{0.6}O_2$ cathode material for lithium ion batteries. *Nano Lett.* **2015**, *15*, 514−522.
(32) Zuo, X.; Fan, C.; Liu, J.; Xiao, X.; Wu, J.; Nan, J. Effect of tris(trimethylsilyl) borate on the high voltage capacity retention of $LiNi_{0.5}Co_{0.2}Mn_{0.3}O_2$/graphite cells. *J. Power Sources* **2013**, *229*, 308−312.
(33) Verma, P.; Maire, P.; Novák, P. A review of the features and analyses of the solid electrolyte interphase in Li-ion batteries. *Electrochim. Acta* **2010**, *55*, 6332−6341.
(34) Dedryvère, R.; Laruelle, S.; Grugeon, S.; Gireaud, L.; Tarascon, J.-M.; Gonbeau, D. XPS identification of the organic and inorganic components of the electrode/electrolyte interface formed on a metallic cathode. *J. Electrochem. Soc.* **2005**, *152*, A689−A696.
(35) Zhou, L.; Dalavi, S.; Xu, M.; Lucht, B. L. Effects of different electrode materials on the performance of lithium tetrafluorooxalato-phosphate (LiFOP) electrolyte. *J. Power Sources* **2011**, *196*, 8073−8084.
(36) Zhang, S. S. A review on electrolyte additives for lithium-ion batteries. *J. Power Sources* **2006**, *162*, 1379−1394.
(37) Larush-Asraf, L.; Biton, M.; Teller, H.; Zinigrad, E.; Aurbach, D. On the electrochemical and thermal behavior of lithium bis(oxalato)-borate (LiBOB) solutions. *J. Power Sources* **2007**, *174*, 400−407.
(38) Andersson, A.; Henningson, A.; Siegbahn, H.; Jansson, U.; Edström, K. Electrochemically lithiated graphite characterised by photoelectron spectroscopy. *J. Power Sources* **2003**, *119−121*, 522−527.
(39) Xie, B.; Lee, H. S.; Li, H.; Yang, X. Q.; McBreen, J.; Chen, L. Q. New electrolytes using Li_2O or Li_2O_2 oxides and tris-(pentafluorophenyl) borane as boron based anion receptor for lithium batteries. *Electrochem. Commun.* **2008**, *10*, 1195−1197.
(40) Chen, Z.; Amine, K. Tris(pentafluorophenyl) borane as an additive to improve the power capabilities of lithium-ion batteries. *J. Electrochem. Soc.* **2006**, *153*, A1221−A1225.
(41) Lin, F.; Nordlund, D.; Weng, T. C.; Zhu, Y.; Ban, C.; Richards, R. M.; Xin, H. L. Phase evolution for conversion reaction electrodes in lithium-ion batteries. *Nat. Commun.* **2014**, *5*, 3358.
(42) Lin, F.; Nordlund, D.; Markus, I.; Weng, T. C.; Xin, H. L.; Doeff, M. Profiling the nanoscale gradient in stoichiometric layered cathode particles for lithium-ion batteries. *Energy Environ. Sci.* **2014**, *7*, 3077−3085.
(43) Lin, F.; Nordlund, D.; Pan, T.; Markus, I. M.; Weng, T. C.; Xin, H. L.; Doeff, M. M. Influence of synthesis conditions on the surface passivation and electrochemical behavior of layered cathode materials. *J. Mater. Chem. A* **2014**, *2*, 19833−19840.
(44) Lin, F.; Markus, I. M.; Doeff, M. M.; Xin, H. L. Chemical and structural stability of lithium-ion battery electrode materials under electron beam. *Sci. Rep.* **2014**, *4*, 5694.
(45) Xu, B.; Fell, C. R.; Chi, M.; Meng, Y. S. Identifying surface structural changes in layered Li-excess nickel manganese oxides in high voltage lithium ion batteries: A joint experimental and theoretical study. *Energy Environ. Sci.* **2011**, *4*, 2223−2233.
(46) Lu, P.; Yan, P.; Romero, E.; Spoerke, E. D.; Zhang, J. G.; Wang, C. M. Observation of Electron-Beam-Induced Phase Evolution Mimicking the Effect of the Charge−Discharge Cycle in Li-Rich Layered Cathode Materials Used for Li Ion Batteries. *Chem. Mater.* **2015**, *27*, 1375−1380.

DOI: 10.1021/acs.chemmater.6b04784
Chem. Mater. 2017, 29, 2141−2149

(47) Shukla, A. K.; Ramasse, Q. M.; Ophus, C.; Duncan, H.; Hage, F.; Chen, G. Unravelling structural ambiguities in lithium-and manganese-rich transition metal oxides. *Nat. Commun.* **2015**, *6*, 8711.
(48) Hy, S.; Su, W. N.; Chen, J. M.; Hwang, B. J. Soft X-ray absorption spectroscopic and raman studies on $Li_{1.2}Ni_{0.2}Mn_{0.6}O_2$ for lithium-ion batteries. *J. Phys. Chem. C* **2012**, *116*, 25242−25247.
(49) Hy, S.; Cheng, J. H.; Liu, J. Y.; Pan, C. J.; Rick, J.; Lee, J. F.; Chen, J. M.; Hwang, B. J. Understanding the Role of Ni in Stabilizing the Lithium-Rich High-Capacity Cathode Material Li $[Ni_xLi_{(1-2x)/3}Mn_{(2-x)/3}]$ O_2 $(0 \leq x \leq 0.5)$. *Chem. Mater.* **2014**, *26*, 6919−6927.

DOI: 10.1021/acs.chemmater.6b04784
Chem. Mater. 2017, 29, 2141−2149